Available online at www.sciencedirect.com

ScienceDirect

Procedia Structural Integrity 76 (2026) 138–144

Structural Integrity Procedia

www.elsevier.com/locate/procedia

5th International Symposium on Fatigue Design and Material Defects FDMD 2025

Experience of defect tolerant design for Additively Manufactured components in high performance cars

Matteo Sepati[a], Giuliano Minerva[b], Luca Patriarca[b], Andrea Vignoni[a], Elia Sbettega[a], Massimo Giannozzi[a], Stefano Beretta[b,c,*]

[a]*Ferrari S.p.A., Viale Enzo Ferrari 27, 41053 Maranello (MO), Italy*
[b]*Politecnico di Milano, Department of Mechanical Engineering, Via La Masa 1, 20156 Milano, Italy*
[c]*Auburn University, National Center for Additive Manufacturing Excellence (NCAME), Auburn, Al 36849, USA*

Abstract

Additive Manufacturing (AM) has rapidly advanced in the motorsport field, enabling the production of custom lightweight components with high-performance alloys. Rapid design iterations and short production lead times make AM ideal to improve component performance. However, predicting fatigue resistance remains challenging due to the inherent presence of manufacturing defects. This work presents the application of a defect-tolerant methodology to predict the impact of manufacturing defects on component performance under operating conditions. First, the manufacturing defects of standard fatigue specimens and a selected component were revealed by X-ray Computed Tomography. Then, machine learning-assisted Extreme Value Statistics was adopted to estimate the occurrence of different defect types in critical regions of the component. Finally, a probabilistic fracture-based design model was applied to quantify the influence of defect size on fatigue performance.

Keywords: Additive Manufacturing; CT scan; Fatigue

Nomenclature

$\Delta\sigma_w$	Endurance limit in presence of a defect
$\Delta\sigma_{w,0}$	Theoretical endurance limit for the defect-free material
$\Delta K_{th,LC}$	Cyclic Stress Intensity Factor at the long crack threshold
$\sqrt{area}$	Defect size expressed with Murakami parameter
$\sqrt{area}_0$	El-Haddad parameter according to the Murakami equivalent crack size
Y	Shape factor

* Corresponding author. Tel.: +39-02-2399-8246
E-mail address: stefano.beretta@polimi.it

2452-3216
10.1016/j.prostr.2025.12.297

1. Introduction

Additive Manufacturing (AM) has shifted the focus from design-for-manufacturing to design-for-performance. In fact, AM opened up the possibility of producing highly complex geometries and optimizing components by strategically placing material only where it is required to withstand external loads. This leads to reduced component mass and enhanced performance, which are key factors for the motorsport industry Leach and Carmignato (2020).

A distinctive feature of racing applications is the extreme pace of design evolution: components are continuously refined, often undergoing hundreds of modifications within a single season. These iterations can be driven by both performance and reliability requirements. As a result, components installed on vehicles can be considered functional prototypes, embedded in an ongoing design–test–racing–redesign loop. In this context, AM proves especially advantageous, drastically shortening the time from concept to track and significantly reducing industrialization costs compared to conventional manufacturing routes.

When geometrical complexity and cost-to-performance considerations justify the use of specific AM technologies, such as Laser Powder Bed Fusion (PBF-LB), it becomes essential to assess how process-inherent defects affect material properties, especially under fatigue loading. In high-performance applications, where components are often designed with minimal safety factors, even small manufacturing defects can trigger unexpected failures.

This work presents the application of defect-tolerant design principles to a high-performance PBF-LB component for racing applications, bridging the flexibility of AM with the stringent reliability demands of motorsport engineering.

2. Methods and Discussion

The specimens and the component used in this work were manufactured by PBF-LB with an Al-based alloy using an SLM 500 system [Nikon SLM Solution Group AG] equipped with four 400 W Yttrium fibre lasers.

In the considered industrial framework, the homologation of AM components follows a two-stage workflow. First, process validation is performed through iterative tuning of printing parameters and material characterization to establish a reproducible process window ECSS-Q-ST-70-80C. Subsequently, product validation is carried out by bench testing to verify compliance with performance and reliability requirements.

For high-performance components, characterized by reduced design safety margins or direct safety implications, this standard workflow is adapted. In addition to process and product validation, a defect-tolerant design methodology is explicitly integrated, enabling more robust lifetime prediction, improved reliability, and the definition of defect acceptability criteria.

For any given material, the defect tolerance framework requires three main ingredients:

1. the calibration of a defect-based fatigue model;
2. the characterization of the defects from a statistical perspective;
3. the use of suitable computational tools for reliability calculations for the design and quality assurance of a component.

2.1. Experimental calibration of the defect-based fatigue model

On the material model side, the fatigue debit induced by defects was evaluated using the Kitagawa-Takahashi (KT) diagram Kitagawa and Takahashi (1976). The bi-linear curve is defined by two asymptotes: the theoretical fatigue strength of defect-free specimens, $\Delta\sigma_{w0}$, and the Stress Intensity Factor (SIF) range threshold for long cracks, $\Delta K_{th,LC}$. The endurance limit $\Delta\sigma_w$ in the short-crack region is usually obtained with the El-Haddad model in terms of Murakami's $\sqrt{area}$ parameter Beretta and Romano (2017), as shown in Fig.1 (a).

The two parameters of the El-Haddad model $\Delta K_{th,LC}$ and $\Delta\sigma_{w,0}$ were obtained with an experimental campaign from standard test specimens, namely Fatigue Crack Growth (FCG) tests with Compact Tension (CT) and Single-Edge Bending (SEB) specimens for $\Delta K_{th,LC}$ and tensile tests for $\Delta\sigma_{w,0}$, as described in Beretta et al. (2022). The predictive capability of the model is first verified with standard high cycle fatigue (HCF) specimens, then a fine-tune calibration is performed by means of micro-notched specimens containing artificial, pre-cracked defects (Fig.1 (b)) larger then the ones naturally occurring on the HCF specimens by adjusting the value of $\Delta K_{th,LC}$.

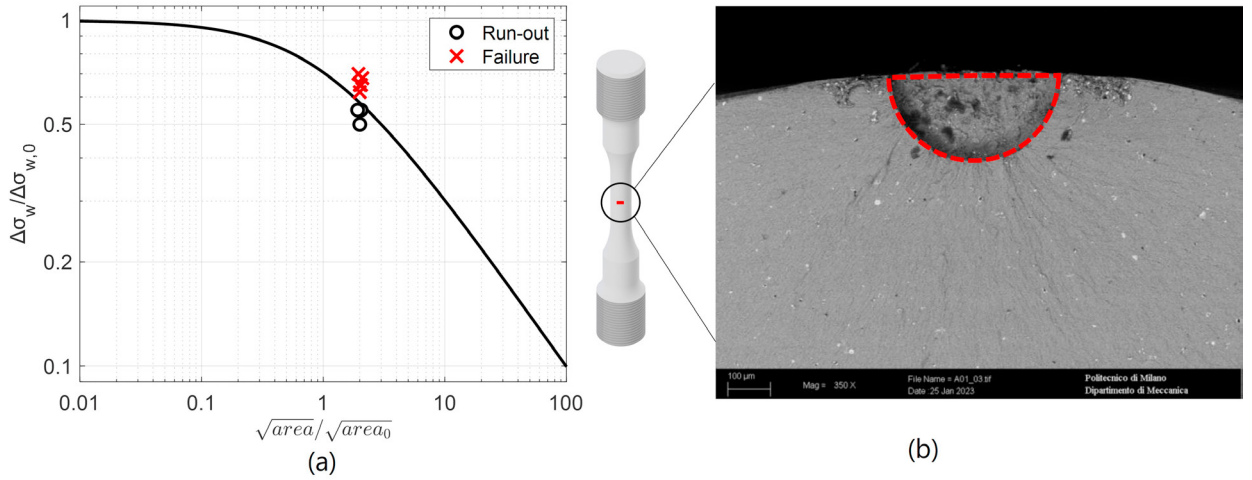

Fig. 1. (a) Scheme of KT diagram with the the El-Haddad model. (b) Micro-notched specimen with a detail of the plunge-Electron Discharge Machining defect.

2.2. *Machine learning-assisted Extreme Value Statistics of volumetric defects*

The statistical characterization of volumetric defects was performed according to the machine learning(ML)-assisted Extreme Value Statistics (EVS) method extensively described in Minerva et al. (2023) and Minerva et al. (2025).

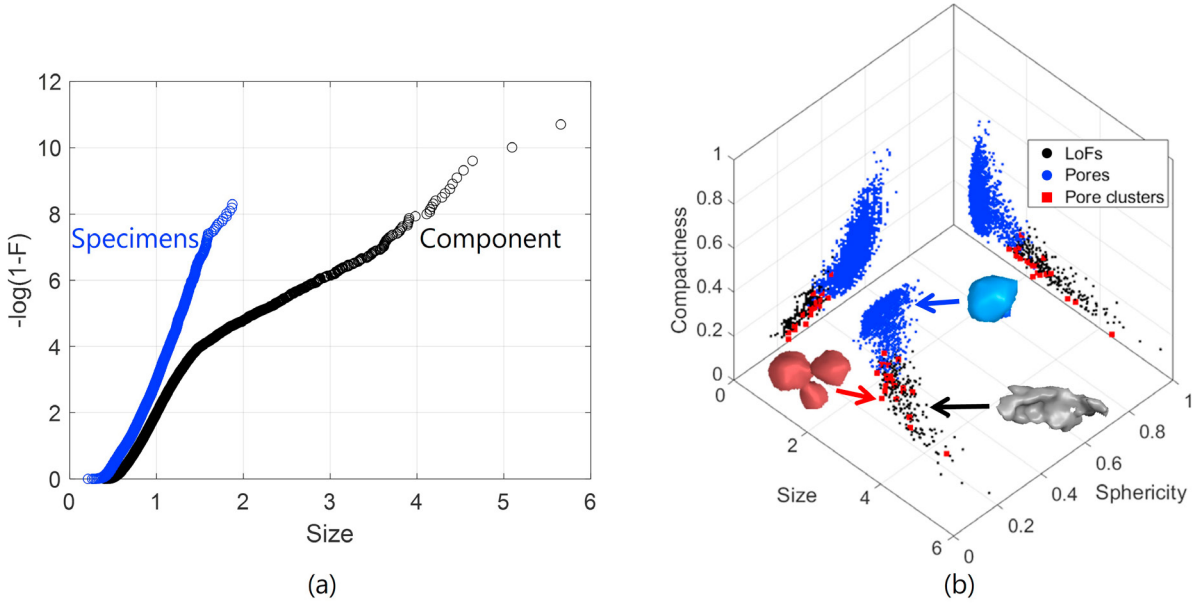

Fig. 2. (a) Comparison between defects population of specimens and components on an exponential probability plot. (b) Size, sphericity and compactness of manually categorized defects from a cut-up of the component.

Micro-focus X-ray Computed Tomography (XCT) scans were performed on the gauge section of nine standard HCF specimens and on a specific component. To achieve a resolution suited for the required defect detectability and

characterization, the component was sectioned in multiple cut-ups and twelve of these cut-ups - spread across the printing volume - were scanned using the set-up reported in the following Tab.1.

Table 1. Details of the set-up of the XCT scan system.

System	Voxel size	Target power	Scan time
Yxlon FF35 CT [Comet Yxlon GmbH]	23 μm	13.6 W	220 min

Internal defects revealed by XCT were analysed with VGSTUDIO MAX 2023.3.1 using the EasyPore algorithm.

Size, expressed as Murakami $\sqrt{area}$ parameter for the projected area perpendicular to the build direction, was retrieved from the identified defects in order to compare the overall distributions between the specimens and the component. Fig. 2 (a) shows the defects size from XCT analysis for all the investigated HCF specimens and the cut-ups of the component on an exponential probability plot. The distributions of defects were significantly different, suggesting that a specimens-centred characterization was not enough to fully capture the material behaviour.

Several shape descriptors were thus extracted from the XCT data of the component with the aim of categorizing the defects. Manual categorization was carried out on one cut-up of the component and three types of defects were observed, namely gas entrapped pores, clusters of pores and lack-of-fusions (LoFs). The seven most impacting shape descriptors, ranked with the ANOVA algorithm, were employed for the categorization, namely: ellipsoidity, size, sphericity, sparseness, roundness, aspect ratio and compactness. The definition for the shape descriptors is provided in Minerva et al. (2023).

Fig. 2 (b) shows some relevant shape descriptors for the manually categorized defects. Lack-of-fusion defects, depicted as black dots, and pore cluster defects, depicted as red squares, significantly overlapped. Therefore, pore clusters were assimilated into the LoFs class and only two classes, pores and LoFs, were adopted for the training of the ML algorithm. The training was performed using MATLAB classification learner tool on an optimizable Neural Network.

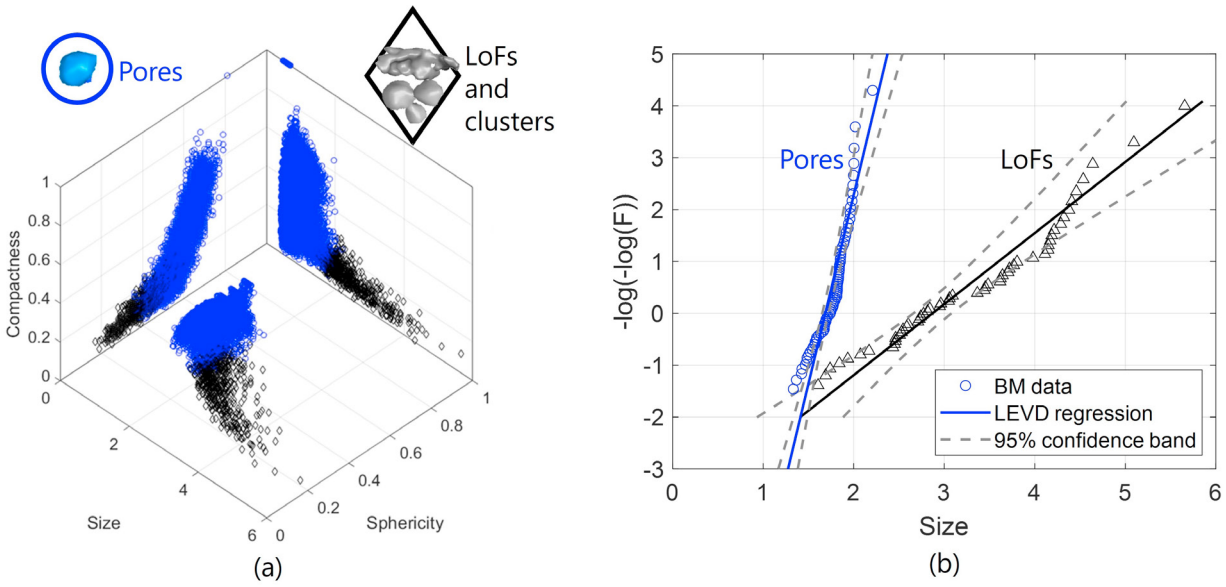

Fig. 3. (a) Size, Sphericity and Compactness of all defects revealed by XCT scan on the cut-ups after categorization with the ML algorithm. (b) Maxima defect size distributions on a Gumbel probability chart after categorization.

The defects of the remaining cut-ups were then categorized using the trained algorithm. The results are shown in Fig. 3 (a), in which it is possible to see how the classification provides a clear distinction of the defect distributions, with pores represented as blue circles and irregular defects (i.e. pore clusters and LoFs) as black diamonds.

While the use of an ML algorithm allows to significantly improve the categorization process, an important limitation to consider is that the trained algorithm is valid only for the specific combination of material, processing parameters and XCT measurements set-up.

After the defects were categorized, Extreme Value Statistics (EVS) was employed to obtain the maxima defects distribution for pores and LoFs. Two different sampling strategies were employed to this end, namely Block Maxima (BM) and Peaks-Over-Threshold (POT) Beretta (2021). The BM data was fit to a Gumbel distribution, reported in Fig. 3 (b), which has cumulative distribution function:

$$F(x) = \exp\left(-\exp\left(-\frac{x-\lambda}{\delta}\right)\right) \tag{1}$$

being λ and δ the parameters of the distribution.

The POT data was fit to an exponential distribution, which has cumulative distribution function:

$$F(x) = 1 - \exp\left(-\frac{x-u}{\sigma}\right) \tag{2}$$

being u and σ the parameters of the distribution.

The distributions obtained with POT and BM were employed to estimate the max characteristic sizes of pores and LoFs for all the cut-ups of the component. The maximum characteristic defect $\hat{x}$ for a volume V_{ref} for the Gumbel distribution is:

$$\hat{x}_{Gumbel} = \lambda + \delta \cdot \log(V_{ref}/V_{BM}) \tag{3}$$

while for the exponential distribution is:

$$\hat{x}_{Exp} = u + \sigma \cdot \log(\rho \cdot V_{ref}) \tag{4}$$

where ρ is the average defect density. Local defect density may be used as well, if it is known for the volume of interest V_{ref}. On the other hand, no effect of local defect density can be considered for the Gumbel distribution and the average defect density of all the cut-ups is assumed uniform for any volume.

Fig. 4(a) provides a comparison between the estimated max characteristic sizes and the maximum defect detected by XCT scan for each cut-ups. The distribution of defects with respect to the component position on the build plate is shown in Fig. 4(b), which clearly depicts how the density of both pores and LoFs changes significantly throughout the platform. For pores, present in all the cut-ups with similar dimensions, both BM and POT sampling resulted suitable. On the other hand, LoFs were characterized by non-uniform spatial distribution, tending to cluster in some regions and be absent or sparse in others. As a consequence, volume driven estimation with the Gumbel distribution were significantly different from the actual maximum defect size, while the maximum characteristic size estimate with the exponential distribution were more accurate.

Fig. 4 (b) shows also an accumulation of LoFs in the upper-left side. This was linked to an improper setup of the nozzles of the gas flow, which produced turbulence and thus induced the creation of the anomalies. By properly tuning the nozzle the issue was subsequently drastically reduced.

While this work focused only on volumetric defects, it is important to underline that in absence of effective surface treatments, surface defects are extremely relevant for fatigue. In particular, the effect of increase in surface roughness with increasing orientation angle with respect to the build direction has to be properly characterized.

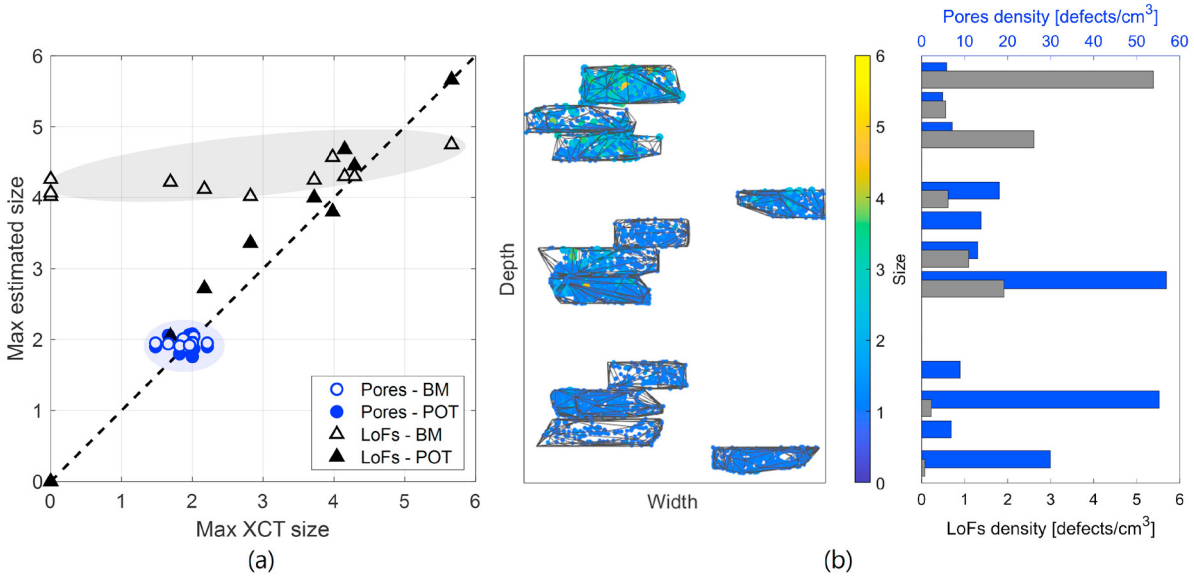

Fig. 4. (a) Comparison between maximum characteristic defect size estimated with BM and POT and actual size of the largest defect revealed by CT scan for each cut up. (b) Differences in the density of pores and LoFs across the build platform for the investigated cut ups. The build direction is perpendicular to the width and depth.

2.3. Design and quality assurance of components

The design methodology and the qualification procedure of AM components, relied on the calibration of the defect-based fatigue model and the statistical characterization of the population of defects as shown in Fig. 5.

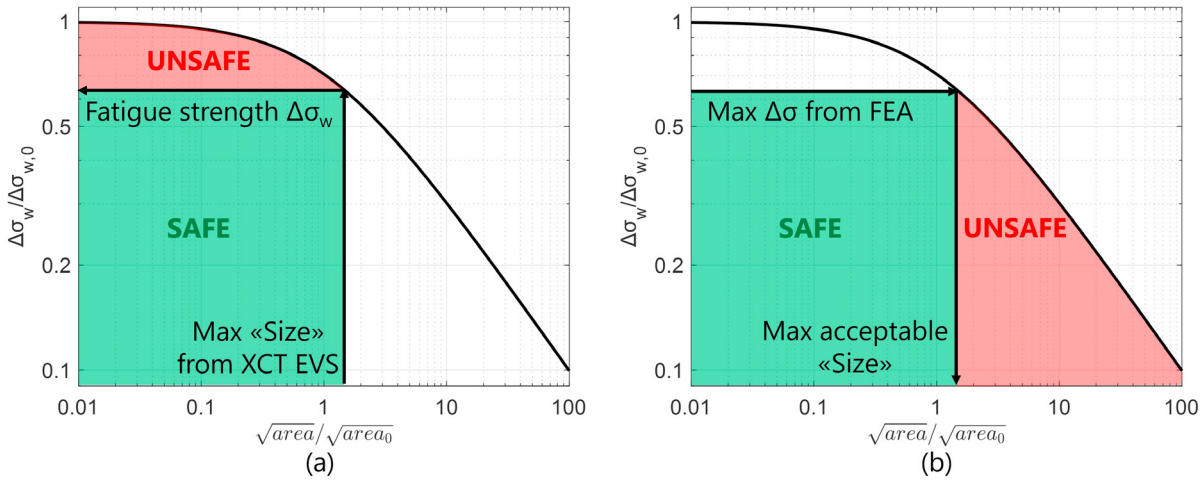

Fig. 5. Exemplary use of Kitagawa-Takahashi diagram and CT scan data for: (a) component design; (b) quality assurance of the production process of the component.

From a design perspective, it is possible to exploit the KT diagram to estimate the endurance limit $\Delta\sigma_w$ for the maximum defect that could occur in a certain material volume.

Two approaches could be applied to this end:

- define the endurance limit associated with the maximum defect occurring in the V_{90} of the component, i.e. the volume of the component that experience a maximum principal stress from 90% to 100% of the largest maximum principal stress.
- divide the component in sub-volumes, define for each sub-volume the maximum defect size and then calculate the associated endurance limit stress.

While the implementation of the V_{90} approach is straightforward, it may be non-conservative in the definition of the maximum defect size. Therefore the sub-volumes approach was ultimately adopted via an in-house routine linked to a Finite Element Analysis (FEA) software, similar to the ProFACE software Sausto et al. (2022), so that different stress ratios and local temperatures could also be properly taken into account.

From a qualification perspective, it is possible to assess the maximum admissible defect size in each position depending on the local stress obtained from FEA, thus creating a defect acceptability map. The process was automated by overlapping the mask of acceptable defects with the post-processing analysis of CT scans for each component in production. This provided a fast-response tool to verify compliance of components, ensuring reliability and efficiency in the production workflow.

3. Conclusions

This work dealt with defect tolerance design approaches for an AM component in high performance cars. The following conclusions were drawn:

- A specimen-centred material characterization may not be enough when there are differences in the type of defects between specimens and the actual component.
- POT sampling revealed to be more accurate than BM to estimate defects with significantly different density distribution across the build plate.
- Kitagawa-Takahashi diagram, XCT scan analysis and EVS proved to be invaluable tools for the design and quality assurance phases.

Acknowledgements

The authors would like to acknowledge all those involved in the development of this project at Politecnico di Milano and Ferrari S.p.A, whose expertise and support have been essential to its success.

References

Beretta, S., 2021. More than 25 years of extreme value statistics for defects: Fundamentals, historical developments, recent applications. International Journal of Fatigue 151, 106407. doi:10.1016/j.ijfatigue.2021.106407.

Beretta, S., Patriarca, L., Gargourimotlagh, M., Hardaker, A., Brackett, D., Salimian, M., Gumpinger, J., Ghidini, T., 2022. A benchmark activity on the fatigue life assessment of AlSi10Mg components manufactured by L-PBF. Materials & Design 218, 110713. doi:10.1016/j.matdes.2022.110713.

Beretta, S., Romano, S., 2017. A comparison of fatigue strength sensitivity to defects for materials manufactured by AM or traditional processes. International Journal of Fatigue 94, 178–191. doi:10.1016/j.ijfatigue.2016.06.020.

ECSS-Q-ST-70-80C, 2021. Space product assurance - Processing and quality assurance requirements for metallic powder bed fusion technologies for space applications.

Kitagawa, H., Takahashi, S., 1976. Application of fracture mechanics to very small cracks or the cracks in the early stage, in: 2nd International Conference on Mechanical Behaviour of Materials.

Leach, R., Carmignato, S., 2020. Precision metal additive manufacturing. CRC Press.

Minerva, G., Awd, M., Koch, A., Walther, F., Beretta, S., 2025. Transferability of anomaly data to fatigue properties of pbf-lb alsi10mg parts with different volumes. International Journal of Fatigue 195, 108852. doi:10.1016/j.ijfatigue.2025.108852.

Minerva, G., Awd, M., Tenkamp, J., Walther, F., Beretta, S., 2023. Machine learning-assisted extreme value statistics of anomalies in alsi10mg manufactured by l-pbf for robust fatigue strength predictions. Materials & Design 235, 112392. doi:10.1016/j.matdes.2023.112392.

Sausto, F., Romano, S., Patriarca, L., Miccoli, S., Beretta, S., 2022. Benchmark of a probabilistic fatigue software based on machined and as-built components manufactured in alsi10mg by l-pbf. International Journal of Fatigue 165, 107171. doi:10.1016/j.ijfatigue.2022.107171.